



HAL
open science

Chiral supramolecular gold-cysteine nanoparticles: Chiroptical and nonlinear optical properties

Isabelle Russier-Antoine, Franck Bertorelle, Alexander Kulesza, Antonin Soleilhac, Amina Bensalah-Ledoux, Stephan Guy, Philippe Dugourd, Pierre-Francois Brevet, Rodolphe Antoine

► To cite this version:

Isabelle Russier-Antoine, Franck Bertorelle, Alexander Kulesza, Antonin Soleilhac, Amina Bensalah-Ledoux, et al.. Chiral supramolecular gold-cysteine nanoparticles: Chiroptical and nonlinear optical properties. Progress In Natural Science-materials International, 2016, 26 (5), pp.455-460. 10.1016/j.pnsc.2016.08.008 . hal-02289459

HAL Id: hal-02289459

<https://univ-lyon1.hal.science/hal-02289459>

Submitted on 22 Jan 2021

HAL is a multi-disciplinary open access archive for the deposit and dissemination of scientific research documents, whether they are published or not. The documents may come from teaching and research institutions in France or abroad, or from public or private research centers.

L'archive ouverte pluridisciplinaire **HAL**, est destinée au dépôt et à la diffusion de documents scientifiques de niveau recherche, publiés ou non, émanant des établissements d'enseignement et de recherche français ou étrangers, des laboratoires publics ou privés.



Distributed under a Creative Commons Attribution - NonCommercial - NoDerivatives 4.0 International License



Original Research

Chiral supramolecular gold-cysteine nanoparticles: Chiroptical and nonlinear optical properties



Isabelle Russier-Antoine, Franck Bertorelle, Alexander Kulesza, Antonin Soleilhac, Amina Bensalah-Ledoux, Stephan Guy, Philippe Dugourd, Pierre-François Brevet, Rodolphe Antoine*

Univ Lyon, Université Claude Bernard Lyon 1, CNRS, Institut Lumière Matière, F-69622, Villeurbanne, France

ARTICLE INFO

Keywords:

Gold
Cysteine
Supramolecular chemistry
Nanoparticles
Chirality
Nonlinear optics

ABSTRACT

Cysteine is a sulfur-containing amino acid that easily coordinates to soft metal ions and grafts to noble metal surfaces. We report a simple synthetic approach for the production of chiral gold-cysteine polymeric nanoparticles soluble in water. Conjugation of cysteine with gold in a polymeric way, leading to ~50 nm diameter nanoparticles, resulted in the generation of new characteristic circular dichroism (CD) signals in the region of 250–400 nm, whereas no CD signal changes were found with cysteine alone. We also investigate their nonlinear optical properties after two-photon absorption. Two-photon emission spectra and first hyperpolarizabilities, as obtained by the hyper-Rayleigh scattering technique, of these particles are presented.

1. Introduction

The chemistry of the sulfur-gold bond [1] is extremely rich and leads to hybrid materials. Such materials encompass gold thiolate coordination oligomers, for instance, $[\text{Au}(\text{I})(\text{SR})_n]$ where SR stands for a chemical group containing a sulfur atom [2] and atomically well-defined clusters $[\text{Au}_n\text{SR}_m]$ [3], to thiols monolayer protected gold nanoparticles (NPs) or supramolecular assemblies like Au(I)(SR) NPs [4] and at the macroscopic level, to flat surfaces. The valence state of gold atoms is expected indeed to have a significant influence on material properties based on gold nanoparticles. While, the majority of gold atoms in nanoparticles are in the Au(0) state under strong reducing conditions, gold atoms in supramolecular assemblies like Au(I)(SR) NPs are in the gold(I) state [5]. As a result, in atomically well-defined clusters of the $[\text{Au}_n\text{SR}_m]$ stoichiometry, a subtle balance between the Au(0) core and the Au(I)–SR shell leads to fascinating material properties and in particular to highly tunable optical properties [6].

Polymeric Au(I) thiolates, with a linear RS–Au–SR motif, are well-known intermediates observed during nanocluster synthesis. Large polymeric Au(I)(SR) NPs with sizes around 100–150 nm are quickly formed after mixing glutathione (GSH)- with Au^{3+} ions [5]. The dissociation of these large polymeric Au(I) thiolates is then a simple route to produce luminescent gold nanoparticles with mixed valence

states [5]. On the other hand, large polymeric Au(I) thiolates can lead to supramolecular nanostructures with diverse morphologies ranging from strings to lamellar structures [7–9]. These structures present UV–visible absorption spectra with the characteristic features of ligand-to-metal (LMCT) and metal-centered charge transfer (MCCT) transitions [10]. Both absorption and emission properties were found to be sensitive to the coordination environment. In particular, the photoemission from MCCT transitions are proofs of Au(I)–Au(I) aurophilic interactions between Au(I) atoms [10]. The sensitivity of the optical properties to the coordination environment was recently used as a time-resolved method for the in situ monitoring of the self-assembly of Au(I)–thiolate NPs [7].

Besides versatile absorption and emission properties of supramolecular Au(I)(SR) NPs, chiral nanostructures of coinage metals with observable optical activity have been successfully engineered [11]. This was for example achieved by adding a chiral center in thiolated ligands. For instance, SH-containing amino acids and peptides such as cysteine (Cys), homocysteine (HCys) and glutathione (GSH) are good candidates to produce such hybrid materials with strong chiroptical properties [12,13]. Circular dichroism methods can thus be used for probing L-cysteine in biological fluids on the basis of chiral nanoparticle [14]. Chirality may also play a critical role for enhancing nonlinear optical properties and thus can be of particular importance for 2 photon biosensing and bioimaging, such as circular dichroism second harmo-

Peer review under responsibility of Chinese Materials Research Society.

* Corresponding author.

E-mail address: rodolphe.antoine@univ-lyon1.fr (R. Antoine).

<http://dx.doi.org/10.1016/j.pns.2016.08.008>

Received 31 July 2016; Accepted 16 August 2016

Available online 22 September 2016

1002-0071/ © 2016 Chinese Materials Research Society. Published by Elsevier B.V. This is an open access article under the CC BY-NC-ND license (<http://creativecommons.org/licenses/by/4.0/>).

nic generation [15]. Nonlinear chiroptical effects of precisely designed chiral plasmonic nanomaterials can be much stronger than such effects observed in the linear regime [16,17]. For atomically well-defined Au_nSR_m clusters, the substitution of achiral by chiral ligands was demonstrated as an efficient strategy to induce significant second-order NLO effects to otherwise centrosymmetric clusters [18,19]. To our knowledge, there is no report available on the nonlinear optical properties (NLO) of large supramolecular NPs like Au(I)(SR) NPs. We hereby report a simple synthetic route to produce such supramolecular polymeric NPs with L- and D-cysteine as the thiolated ligand. Chiroptical and nonlinear optical properties, i.e. two-photon emission spectra and first hyperpolarizabilities of these particles are presented.

2. Experimental and methods

2.1. Materials

All the chemicals were commercially available and used as received. Tetrachloroauric(III) acid trihydrate ($HAuCl_4 \cdot 3H_2O$) was purchased from Acros Organics, L- and D-cysteine and racemic DL-cysteine (L- and D-Cys, and DL-Cys), triethylamine (TEA) and glacial acetic acid, methanol (MeOH), diethyl ether (Et_2O) were purchased from Sigma-Aldrich. Ultrapure water with specific resistivity of 18.2 M Ω was used throughout the synthesis.

2.2. Size characterization

Hydrodynamic particle diameters were measured by dynamic light scattering (DLS) using a Malvern Zetasizer Nano ZS. A 633 nm wavelength laser beam was sent to an infinitely diluted sample maintained at 25 °C and the scattered signal intensity was analyzed at a 173° angle. DLS allowed access to the particle average sizes and the broadness of the size distribution indicated by the poly value. The higher this poly value, the broader the size distribution is. The cumulant analysis method was used.

2.3. X-ray Photoelectron Spectroscopy (XPS)

XPS measurements were carried out using a PHI Quantera SXM instrument (Physical Electronics, Chanhassen, USA) equipped with a 180° hemispherical electron energy analyzer and a monochromatized Al K α (1486.6 eV) source operated at 15 kV and 4 mA. The analysis spot had a diameter of 200 μ m and the detection angle relative to the substrate surface was 45°.

2.4. UV-visible, fluorescence and circular dichroism measurements

UV-vis spectra in solution were recorded using an AvaSpec-2048 fiber optic spectrometer and an AvaLight-DH-S deuterium-halogen light source. Fluorescence excitation and emission spectra were obtained using a Fluoromax-4 Horiba fluorimeter. CD spectra were recorded using a home-made setup based on Photo Elastic Modulator and lock-in amplifier detection devices previously described in Ref. [20].

2.5. Nonlinear optical measurements

The set-up for hyper-Rayleigh scattering (HRS) and two-photon emission (TPE) has been described in details in previous works [21–23]. Briefly, the light source for the HRS and TPE measurements was a mode-locked femtosecond Ti: sapphire laser delivering at the fundamental wavelength of 780 nm and 950 nm pulses with a duration of about 140 fs at a repetition rate of 80 MHz. After passing through a low-pass filter to remove any unwanted harmonic light generated prior to the cell, the fundamental beam of about 300 mW was focused by a low numerical aperture microscope objective into a 0.5 cm spectro-

photometric cell containing the aqueous solutions. The HRS and two-photon emission fluorescence (TPEF) light were collected at an angle of 90° from the incident direction by a 2.5 cm focal length lens. The HRS light was separated from the excitation light by a high-pass filter and a monochromator set at the second harmonic wavelength. The HRS light was then detected with a photomultiplier tube working in the single photon counting regime. For the TPE signal, the wavelength of the spectrometer (iHR320 spectrometer) was scanned between 350 nm and 750 nm but the same detection unit was used.

2.6. Computational

Structural and optical properties of gold-cysteinate complexes have been explored theoretically using density functional theory (DFT) and time dependent DFT (TDDFT) calculations as implemented in Gaussian09 [24]. For geometry optimizations the B97D functional [25] including dispersion corrections was used together with Ahlrichs def2-SVP basis set and the appropriate scalar relativistic effective core potential [26]. For the calculation of excited states, the hybrid long-range corrected functional ω B97X-D was used [27]. Oligomers of Au-Cys were optimized using the PM7 semi-empirical Hamiltonian implemented in the MOPAC2012 code [28].

3. Results and discussion

3.1. Synthesis

Au-Cys complexes (L-, D- and racemic) were directly prepared in a 25 ml centrifuge tube. Briefly, 0.38 mmol of cysteine (D- or L-) is dissolved in 20 ml of water and 0.5 ml of triethylamine. 0.5 ml of gold salt (0.127 mmol, 50 mg) is quickly added and the solution is stirred 30 s by inversion (the color becomes slightly yellow). Quickly, 1 ml of glacial acetic acid is added to induce precipitation of Au-Cys which is centrifuged (5 mn/6000 rpm). The supernatant is removed and Au-Cys is redispersed in water (2 ml with 100 μ l of TEA, vortex time 5 mn). 20 ml of methanol is then added to precipitate Au-Cys with centrifugation (10 mn/6000 rpm). Au-Cys was also redispersed in 2 ml of water with 10 μ l of TEA and precipitated with MeOH (10 ml)/ Et_2O (10 ml). After centrifugation (10 mn/6000 rpm), the product is dried in air. For the experiment, the resulting powder is dissolved in water containing 0.1% v/v of TEA.

3.2. Characterization of gold-cysteine NPs

The as-prepared gold-L-cysteine NPs were found to be stable at room temperature for several weeks. The straightforward protocol produced a pure nanomaterial without the need for size separation and achieves large yields (Fig. 1a). A yellow, non-luminescent powder was obtained in this case. The product could be dried and fully redispersed in water with no loss of material or change in chemical identity. Fig. 1b shows the size distributions of the gold-L-cysteine NPs in aqueous solutions obtained by DLS. Only one component with a mean hydrodynamic diameter (HD) of 50 ± 11 nm was observed. Quantitative XPS measurements indicated an Au: Cys ratio close to a 1:1 stoichiometry in gold-cysteine NPs (see Table S1 and Fig. S1). We also used XPS to investigate the valence state of the gold atoms in the NPs. XPS spectra of 20 nm colloidal Au(0) NPs standard and polymeric GS-Au(I) thiolates were obtained showing that the Au 4f $_{7/2}$ binding energies (BE) are 83.8 and 85.0 eV, respectively [5]. As shown in Fig. 1c, Au 4f $_{7/2}$ binding energy (BE) of the gold-L-cysteine NPs is 84.8 eV, which is close to that of Au(I) (BE 85.0 eV) in polymeric GS-Au(I) NPs, suggesting the existence of Au(I) in our NPs. Similar results were obtained for D-CysNPs (data not shown).

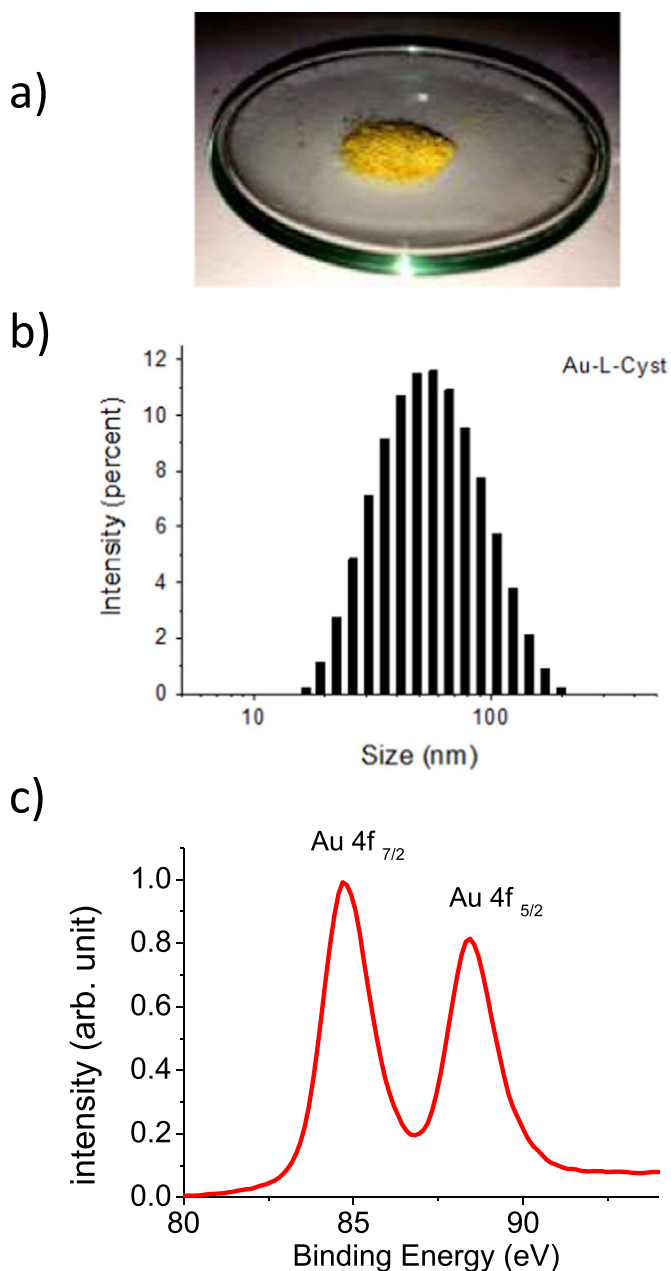


Fig. 1. a) Photograph representing the orange colored powder (~ 1/4 g) due to the gold-cysteine NPs, b) hydrodynamic diameters of the gold-L-cysteine NPs in aqueous solution, c) Au 4f binding energy (BE) of the gold-L-cysteine NPs.

3.3. Linear optical and chiroptical properties

Because of the strong complexation ability of sulfur-containing cysteine anions (RS⁻) toward Au(I), the interaction of Ag(I) with Cys occurs immediately. This is indicated by the appearance of a strong absorption band at 365 nm, a spectral range in which both Cys and Ag(I) are optically transparent (Fig. 2). This absorption band is very close to the one reported for Au(I)-thiolate or Au(I)-Cys supramolecular nanostructures [8,29]. This further suggests that the NPs are of Au(I)(SR) polymeric nature. Absorption spectra of Au(I)-L-Cys and Au(I)-D-Cys solutions are almost the same, as shown in Fig. S2.

The CD spectra recorded in the spectral region corresponding to the characteristic absorption are shown in Fig. 2 and feature a remarkably strong CD signal. As expected, they show perfect mirror images for the two enantiomers. Spectra are characterized by a strong and well defined CD band at 368 nm (21 nm FWHM) positive (negative) for

the L (D) enantiomer and a broad less structured signal at lower wavelengths. These CD bands occur at wavelengths at which the aurophilic-interaction-related LMCT transition absorbs, meaning that the Au-S interface formed by complexation carries chiral information in some way. It can be noted that NPs were synthesized using the same procedure with the racemic D,L cysteine ligand molecule. A NPs diameter of 220 nm was obtained. While optical spectra were similar to those for Au-L-Cys and Au-D-Cys NPs, no CD signal was observed in the region of 250–400 nm as seen in Fig. S3.

In term of chiroptical intensity, the asymmetric g factor (defined as $\Delta \text{Abs}/\text{Abs}$) reaches the maximum value of $\sim 3.5 \cdot 10^{-3}$ at 374 nm (see Fig. 2). This value is similar to what is measured for helicene-like molecules specially designed for strong chiroptical activity [30]. This strength cannot be explained by some coupling between Cys chiral centers and LMCT bands. Indeed, the Cys chiral center (one saturated CH₂ see Fig. 3) is not overlapping with the S-Au group neither spatially, nor spectrally (CD transitions of Cys occurs at λ below 210 nm, 150 nm away from the main peak of the (Au-L/D Cys)_n CD spectra. The strong CD bands may likely found their origin in a geometrical structure which couples together the S-Au bond localized LMCT transitions in a chiral way. This may be an indication of the synergetic interplay of the electrostatic interaction among the –SR side chains and the Au(I)–Au(I) aurophilic attraction in the Au(I)-Cys polymeric backbone, which likely may result in some helicity, as proposed by Jiang and co-workers for Ag(I)-Cys nanostructures [31]. According to the literature, the (AuSR)_n polymers are held together by bridging thiol groups [32,33].

In order to demonstrate that the hypothesized helical structural motifs may be straightforwardly formed upon complexation of Au(I) with cysteinate and that they might be responsible for the measured strong electronic circular dichroism (ECD) signals, the prototype structural models were set up using electronic structure calculations at the DFT and semi-empirical level. We have constructed Au-Cys complexes so that they meet the requirement for a) the presence of an optical transition with contribution from excitation within the Au-S unit, b) a strong electronic circular dichroism signal and c) providing the possibility to form ordered polymeric structures. The results of this exploration of structural and optical properties are given in Fig. 3 and Fig. S4. We started with the zwitterionic cysteinate attached to a Au(I) ion. This complex absorbs according to calculations at around 350 nm but with no pronounced ECD features (Table S2). The absence of ECD activity confirms that the Au-S unit near the chiral center of the cysteine alone is unlikely to be responsible for the observed CD activity in the polymer. We optimized the cysteinate-sandwiched Au(I) ion as model for the S-Au-S motif in the polymer. The additional Au-S bond results in an increase of the transition energy to about 225 nm and indeed a weak ECD activity emerges (Table S2). Adding more gold ions to this base motif increased the ECD intensity (See Fig. S4 and Table S2), while generated a Au-S-Au-S-Au conformation-dependent pattern (comparing the different ECD signals for the three possible Au-S-Au-S-Au units is shown in Table S2). Indeed, the axis orientation of the central S-Au-S bond is chiral itself and displays a tilt angle with regard to the axis of the biomolecular template. The direction of this tilt is induced by the preferential conformation of either L or D cysteine in the hydrogen-bonded dimer. Also we calculated the ECD rotatory strengths of the D-cysteine based enantiomer, confirming that it is the mirror image of the L-cysteine-based enantiomer and suggesting that the biomolecular template imprints the chirality information to the S-Au bond. Moreover, the nature of the electronic transition mainly located at the S-Au unit (Au 5d-6s combined with contribution of the ligand, in particular sulfur's p orbital) as shown by the natural transition orbitals in Fig. S4, and thus fully compatible with the assignment as the MLCT transitions. These simple models confirm that optical excitation of Au-S unit placed in an appropriate chiral environment gives rise to strong ECD signals as recorded experimentally. In order to judge the potential to form polymeric materials under

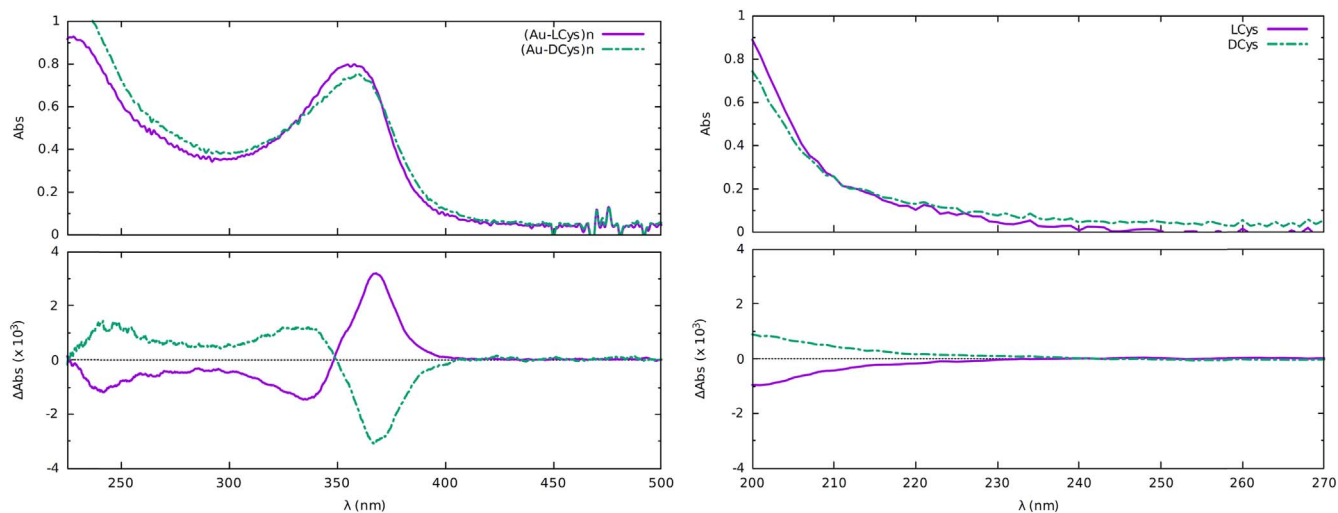


Fig. 2. Absorption (top) and CD (bottom) spectra of cysteine amino-acid and Au-Cys NPs.

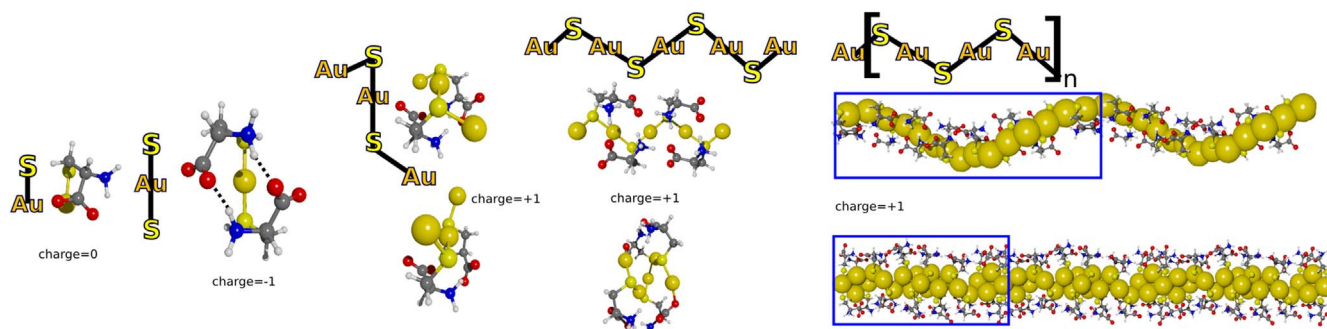


Fig. 3. Structures of hypothesized helical S-Au-S motifs complexed by Cysteine. From left to right: DFT optimized structures of Au-Cys (Cysteinate-gold complex), Cys-Au-Cys, Au-(Cys-Au)₂, Au-(Cys-Au)₃ and structural model of helical Au-Cys polymers (blue box shows the PM7 optimized oligomers of the two prototype complexes I and II, repeated along the main axis). Charge states in the calculations defined by Au-Cys stoichiometry as indicated next to the structures. (For interpretation of the references to color in this figure legend, the reader is referred to the web version of this article.)

retention of chiral Au-S motifs, we optimized oligomers composed of the DFT-optimized complexes Au(Cys-Au)_{2,3} at the PM7 level of theory. Notice that the applicability of semi-empirical Hamiltonians to describe the bonding of gold is limited, but in this case, geometries of the base complex are very similar to the DFT optimized one. These oligomers appear to support helical motifs because the strong hydrogen bonding imposes a tilt-angle onto the S-Au-S unit. In the so-obtained helical polymer models, either the organic ligand acts like a cast for a closely arranged gold core or with more monomers per turn, the helix can be composed of parallel Cys and Au strands.

3.4. Nonlinear optical properties

Two-photon excited fluorescence spectrum with an excitation at 800 nm was recorded for the as-prepared Au-L-cysteine NPs as shown in Fig. 4. A broad band in the visible range between 400 and 700 nm and centered at about 480 nm was observed. A similar spectrum was obtained for the Au-D-cysteine NPs (Fig S5). Interestingly, the NPs are non-fluorescent with a one-photon excitation between 300 and 400 nm whereas an intense two-photon excitation fluorescence spectrum was observed. One photon excited photoemission was attributed to MCCT transitions arising from Au(I)–Au(I) aurophilic interactions between the Au(I) atoms. Lack of photoemission probably means that the supramolecular structure adopted by the Au-Cys polymer leads to a large Au–Au distance precluding MCCT transitions arising from Au(I)–Au(I) aurophilic interactions to occur. Two-photon excited fluorescence occurs through different relaxation mechanisms. The difference observed between the one photon excited fluorescence (OPEF) and TPEF

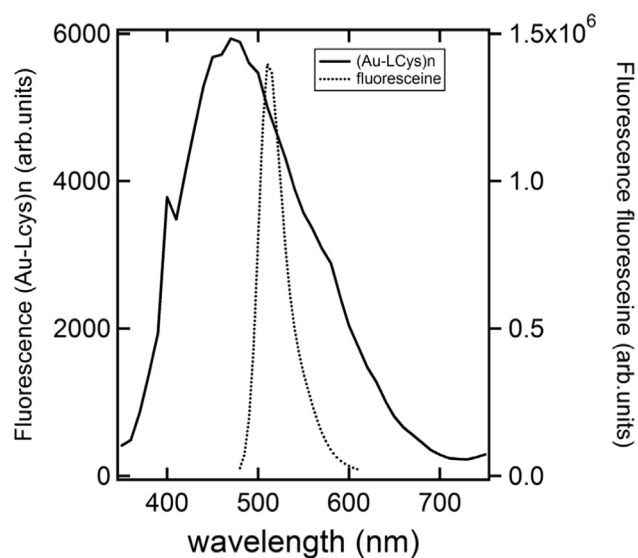


Fig. 4. Two-photon emission spectrum for Au-L-cysteine NPs as a function of wavelength for an excitation wavelength at 800 nm. For comparison, the TPE spectrum of fluorescein (at a concentration of 10 μM) is given.

spectra may therefore be accounted for the different symmetry rules required for the MCCT excitations between Au atoms and the LMCT excitations as already observed for Ag nanoclusters [21].

First hyperpolarizability of the as-prepared gold-L-cysteine NPs was

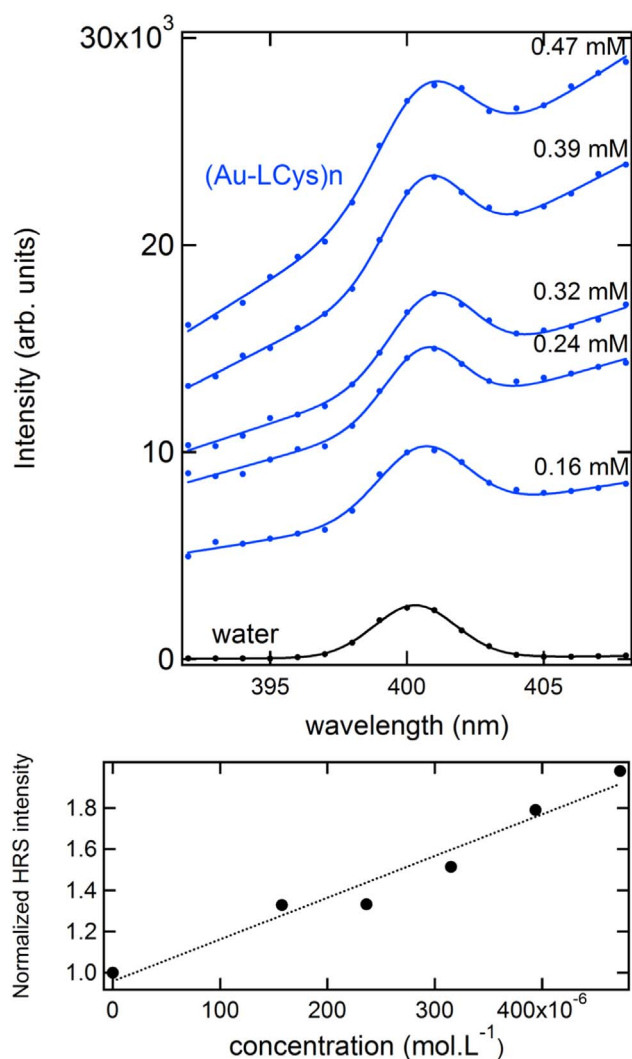


Fig. 5. (Top panel) HRS intensity versus wavelength of Au-L-cysteine NPs solutions of different concentrations (blue circles). Line: fit to a Gaussian function superposed on a linearly increasing function of the wavelength. (bottom panel) Plot of the HRS intensity for Au-L-cysteine as a function of concentration. The continuous lines correspond to the linear adjustment to Eq. (1). (For interpretation of the references to color in this figure legend, the reader is referred to the web version of this article.)

also obtained using the hyper-Rayleigh scattering (HRS) technique. The HRS intensity was recorded for several concentrations of the gold-L-cysteine NPs dispersed in aqueous solutions (Fig. 5), and short range spectra were recorded around the HRS wavelength. This experimental procedure is deemed necessary to ensure that the process corresponds to the conversion of two photons at the fundamental frequency into one photon at the harmonic frequency. It is observed in particular that the HRS line is located on top of a strong broadband photoluminescence background (Fig. 5). The subtraction of the photoluminescence background was then performed by adjusting the narrow band contribution with a Gaussian function for the HRS line superposed on a linear function of the wavelength accounting for the broadband luminescence background. This subtraction procedure is allowed since the two processes, photoluminescence and HRS, are incoherent.

The HRS intensity normalized by the intensity recorded for neat water is then given by:

$$\frac{I_{\text{HRS}}}{I_{\text{HRS}}^{\text{w}}} = \frac{\langle N_w \beta_w^2 + N \beta^2 \rangle}{\langle N_w \beta_w^2 \rangle} = 1 + b' N \langle \beta^2 \rangle \quad (1)$$

where

Table 1
Quadratic hyperpolarizabilities for the different solutions at 750 nm and 800 nm.

NPs	$10^{30} \cdot \beta / \text{Au-cysteine unit}$ (water=0.087.10 ⁻³⁰ esu) $\lambda_{\text{exc.}}=750 \text{ nm}$	$10^{30} \cdot \beta / \text{Au-cysteine unit}$ (water=0.087.10 ⁻³⁰ esu) $\lambda_{\text{exc.}}=800 \text{ nm}$
Au-LCysNPs	92	29
Au-DCysNPs		28
Au-DLCysNPs	387	116

$$b' = 1/N_w \langle \beta_w^2 \rangle \quad (2)$$

with the subscripts w standing for water, the reference solvent used in this experiment. The losses due to absorption at the fundamental and the harmonic frequency were determined from the separate UV–visible absorption measurements and all data were corrected prior to the analysis. The HRS intensity recorded for different concentrations (N) of NPs in aqueous solution is reported in Fig. 5.

As seen in Eq. (1), it is necessary to know the hyperpolarizability of the bare solvent to determine the hyperpolarizability of the gold-L-cysteine NPs. A discussion on the neat water reference value may be found in a previous work [34]. The hyperpolarizability values obtained for the different solutions for [Au-cysteine] concentrations ranging from 160 μM to 470 μM , are reported in Table 1. The final concentration in terms of Au-L-cysteine NPs is not known. However, the [Au-cysteine] concentration and the atomic Au content are. We therefore only reported the gold-L-cysteine NPs hyperpolarizabilities in units of 10^{30} esu per Au-cysteine unit (Table 1). A similar value was obtained for the Au-D-cysteine NPs. The values reported for the Au-L-cysteine NPs, i.e. 29×10^{-30} esu, is more than two orders of magnitude larger than the values reported for Au NPs in the same size range of 50 nm diameters [22]. On the other hand, an absolute value of only 0.16×10^{-30} esu for the first hyperpolarizability of non-aromatic amino acids was measured by Duboisset et al. [34]. One can therefore speculate that a strong enhancement of the nonlinear optical properties of Au-L- and D-cysteine NPs is due to the S-Au bond and supramolecular polymeric organization. We also performed the HRS measurements for the racemic Au-DL-cysteine NPs that are not chiral, according to the CD spectrum in Fig. S3c. The hyperpolarizabilities in units of 10^{30} esu per Au-cysteine unit for gold-DL-cysteine NPs was found to be 4 times higher than the one obtained for the chiral Au-L-cysteine and Au-D-cysteine NPs (Table 1). It is therefore suggested that the supramolecular organization plays a dominant role as compared to chirality. It has been recently reported that Langmuir-Blodgett films of chiral helicenes composed of supramolecular arrangements yield second-order NLO susceptibilities about 30 times larger for the non-racemic materials than for the racemic one, although with the same chemical structure [35]. However, in the present case, the strong enhancement of the nonlinear optical properties of Au-L- and Au-D-cysteine NPs cannot be ascribed to the chiral properties but rather to the polymeric supramolecular organization. This origin is probably also the reason of the size difference between the chiral and achiral NPs as well as their linear absorption difference. In terms of second order nonlinearity, the symmetry breaking result from the unique structural features of the NPs is probably inducing a bulk response. This is in stark contrast to plasmonic nanoparticles whose NLO properties depend on the shape defects, plasmon enhancement and retardation effects [36]. Interestingly, the reported hyperpolarizabilities increase by decreasing the excitation wavelength from 800 nm to 750 nm. This increase is ascribed to the resonance effect at the second harmonic wavelength, the absorption band lying at 365 nm, close to the harmonic 375 nm. This feature has recently been demonstrated for small silver nanoclusters too [23].

4. Conclusions

In summary, we report a simple synthesis to produce large chiral supramolecular gold-cysteine nanoparticles. Gold-cysteine polymeric NPs present remarkable two-photon nonlinear spectra as compared to their one-photon excited one and very large first hyper-polarizabilities. They appear therefore to be good candidates for nonlinear optical microscopy, either two photon or second harmonic imaging microscopy. Furthermore, an enhanced CD signal is reported for these NPs. Between plasmonic large coinage metal NPs [36] and gold quantum nanoclusters [22] NLO-phores, the chiral supramolecular gold-cysteine polymeric NPs constitute therefore a new class of nanomaterials with chiroptical properties driven by their supramolecular chirality character. Nevertheless, the exact supramolecular architecture remains also an important feature to design efficient quadratic NLO systems due to the major role of the centrosymmetry breaking.

Acknowledgments

The authors would like to thank Céline Brunon from Science et Surface (www.science-et-surface.fr) for XPS spectra. The research leading to these results received funding from the European Research Council under the European Union's Seventh Framework Programme (FP7/2007-2013 Grant agreement N°320659).

Appendix A. Supporting information

Supplementary data associated with this article can be found in the online version at <http://dx.doi.org/10.1016/j.pnsc.2016.08.008>.

References

- [1] E. Pensa, E. Cortés, G. Corthey, P. Carro, C. Vericat, M.H. Fonticelli, et al., *Acc. Chem. Res.* 45 (8) (2012) 1183–1192.
- [2] R.J. Puddephatt, *Chem. Soc. Rev.* 37 (9) (2008) 2012–2027.
- [3] R. Jin, *Nanoscale* 7 (5) (2015) 1549–1565.
- [4] M.-C. Daniel, D. Astruc, *Chem. Rev.* 104 (1) (2004) 293–346.
- [5] C. Zhou, C. Sun, M. Yu, Y. Qin, J. Wang, M. Kim, et al., *J. Phys. Chem. C* 114 (17) (2010) 7727–7732.
- [6] R. Jin, S.-K. Eah, Y. Pei, *Nanoscale* 4 (14) (2012) 4026.
- [7] H. Nie, M. Li, Y. Hao, X. Wang, S.X.-A. Zhang, *Chem. Sci.* 4 (4) (2013) 1852–1857.
- [8] H. Nie, M. Li, Y. Hao, X. Wang, S. Gao, P. Wang, et al., *RSC Adv.* 4 (92) (2014) 50521–50528.
- [9] H. Nie, M. Li, Y. Hao, X. Wang, S. Gao, B. Yang, et al., *J. Colloid Interface Sci.* 434 (2014) 104–112.
- [10] J.M. Forward, D. Bohmann, J.P. Fackler, R.J. Staples, *Inorg. Chem.* 34 (25) (1995) 6330–6336.
- [11] V.K. Valev, J.J. Baumberg, C. Sabilia, T. Verbiest, *Adv. Mater.* 25 (18) (2013) 2517–2534.
- [12] M. Farrag, M. Tschurl, U. Heiz, *Chem. Mater.* 25 (6) (2013) 862–870.
- [13] J. Koktan, H. Sedláčková, I. Osante, C. Cativiela, D. Díaz Díaz, P. Řezanka, *Colloids Surf. A: Physicochem. Eng. Asp.* 470 (2015) 142–148.
- [14] R. Jin, *Nanoscale* 2 (3) (2010) 343–362.
- [15] H. Lee, M.J. Huttunen, K.J. Hsu, M. Partanen, G.Y. Zhuo, M. Kauranen, et al., *Biomed. Opt. Express* 4 (6) (2013) 909–916.
- [16] R. Kolkowski, L. Petti, M. Rippa, C. Lafargue, J. Zyss, *ACS Photonics* 2 (7) (2015) 899–906.
- [17] J. Butet, P.-F. Brevet, O.J.F. Martin, *ACS Nano* 9 (11) (2015) 10545–10562.
- [18] S. Knoppe, H. Häkkinen, T. Verbiest, *J. Phys. Chem. C* 119 (49) (2015) 27676–27682.
- [19] S. Knoppe, M. Vanbel, S. van Cleuvenbergen, L. Vanpraet, T. Bürgi, T. Verbiest, *J. Phys. Chem. C* 119 (11) (2015) 6221–6226.
- [20] S. Guy, A. Stoita-Crisan, A. Bensalah-Ledoux, T. Vautey, L. Guy, *Opt. Mater.* 34 (2) (2011) 347–350.
- [21] I. Russier-Antoine, F. Bertorelle, R. Hamouda, D. Rayane, P. Dugourd, Z. Sanader, et al., *Nanoscale* 8 (5) (2016) 2892–2898.
- [22] I. Russier-Antoine, F. Bertorelle, M. Vojkovic, D. Rayane, E. Salmon, C. Jonin, et al., *Nanoscale* 6 (22) (2014) 13572–13578.
- [23] Z. Sanader, M. Krstic, I. Russier-Antoine, F. Bertorelle, P. Dugourd, P.-F. Brevet, et al., *Phys. Chem. Chem. Phys.* 18 (18) (2016) 12404–12408.
- [24] Frisch MJ, Trucks GW, Schlegel HB, Scuseria GE, Robb MA, Cheeseman JR, et al. *Gaussian 09*. Wallingford, CT, USA; Gaussian, Inc.; 2009.
- [25] S. Grimme, *J. Comput. Chem.* 27 (15) (2006) 1787–1799.
- [26] F. Weigend, R. Ahlrichs, *Phys. Chem. Chem. Phys.* 7 (18) (2005) 3297–3305.
- [27] J.-D. Chai, M. Head-Gordon, *Phys. Chem. Chem. Phys.* 10 (44) (2008) 6615–6620.
- [28] J.J.P. Stewart, *J. Mol. Model.* 19 (1) (2013) 1–32.
- [29] B. Söptei, J. Mihály, I.C. Szgyártó, A. Wacha, C. Németh, I. Bertóti, et al., *Colloids Surf. A: Physicochem. Eng. Asp.* 470 (2015) 8–14.
- [30] A. Bensalah-Ledoux, D. Pitrat, T. Reynaldo, M. Srebro-Hooper, B. Moore, J. Autschbach, et al., *Chem. Eur. J.* 22 (10) (2016) 3333–3346.
- [31] J.-S. Shen, D.-H. Li, M.-B. Zhang, J. Zhou, H. Zhang, Y.-B. Jiang, *Langmuir* 27 (1) (2011) 481–486.
- [32] R.J. Puddephatt, *The Chemistry of Gold*, Elsevier Scientific Publishing Company, Amsterdam, The Netherlands, 1978.
- [33] R. Randazzo, A. Di Mauro, A. D'Urso, G.C. Messina, G. Compagnini, V. Villari, et al., *J. Phys. Chem. B* 119 (14) (2015) 4898–4904.
- [34] J. Duboisset, A. Deniset-Besseau, E. Benichou, I. Russier-Antoine, N. Lascoux, C. Jonin, et al., *J. Phys. Chem B* 117 (34) (2013) 9877–9881.
- [35] T. Verbiest, S.V. Elshocht, M. Kauranen, L. Hellemans, J. Snauwaert, C. Nuckolls, et al., *Science* 282 (5390) (1998) 913–915.
- [36] I. Russier-Antoine, E. Benichou, G. Bachelier, C. Jonin, P.F. Brevet, *J. Phys. Chem. C* 111 (26) (2007) 9044–9048.